

RESEARCH ARTICLE

Flow-compensated diffusion encoding in MRI for improved liver metastasis detection

Frederik B. Laun¹, Tobit Führes¹, Hannes Seuss^{1,2}, Astrid Müller¹, Sebastian Bickelhaupt¹, Alto Stemmer³, Thomas Benkert³, Michael Uder¹, Marc Saake^{1*}

1 Institute of Radiology, University Hospital Erlangen, Friedrich-Alexander-Universität Erlangen-Nürnberg, Erlangen, Germany, **2** Department of Radiology, Klinikum Forchheim—Fränkische Schweiz gGmbH, Forchheim, Germany, **3** Siemens Healthcare GmbH, Erlangen, Germany

* marc.saake@uk-erlangen.de

Abstract

Magnetic resonance (MR) diffusion-weighted imaging (DWI) is often used to detect focal liver lesions (FLLs), though DWI image quality can be limited in the left liver lobe owing to the pulsatile motion of the nearby heart. Flow-compensated (FloCo) diffusion encoding has been shown to reduce this pulsation artifact. The purpose of this prospective study was to intra-individually compare DWI of the liver acquired with conventional monopolar and FloCo diffusion encoding for assessing metastatic FLLs in non-cirrhotic patients. Forty patients with known or suspected multiple metastatic FLLs were included and measured at 1.5 T field strength with a conventional (monopolar) and a FloCo diffusion encoding EPI sequence (single refocused; b-values, 50 and 800 s/mm²). Two board-certified radiologists analyzed the DWI images independently. They issued Likert-scale ratings (1 = worst, 5 = best) for pulsation artifact severity and counted the difference of lesions visible at b = 800 s/mm² separately for small and large FLLs (i.e., < 1 cm or > 1 cm) and separately for left and right liver lobe. Differences between the two diffusion encodings were assessed with the Wilcoxon signed-rank test. Both readers found a reduction in pulsation artifact in the liver with FloCo encoding (p < 0.001 for both liver lobes). More small lesions were detected with FloCo diffusion encoding in both liver lobes (left lobe: six and seven additional lesions by readers 1 and 2, respectively; right lobe: five and seven additional lesions for readers 1 and 2, respectively). Both readers found one additional large lesion in the left liver lobe. Thus, flow-compensated diffusion encoding appears more effective than monopolar diffusion encoding for the detection of liver metastases.

OPEN ACCESS

Citation: Laun FB, Führes T, Seuss H, Müller A, Bickelhaupt S, Stemmer A, et al. (2022) Flow-compensated diffusion encoding in MRI for improved liver metastasis detection. PLoS ONE 17(5): e0268843. <https://doi.org/10.1371/journal.pone.0268843>

Editor: Pascal A. T. Baltzer, Medical University of Vienna, AUSTRIA

Received: December 20, 2021

Accepted: May 9, 2022

Published: May 26, 2022

Copyright: © 2022 Laun et al. This is an open access article distributed under the terms of the [Creative Commons Attribution License](https://creativecommons.org/licenses/by/4.0/), which permits unrestricted use, distribution, and reproduction in any medium, provided the original author and source are credited.

Data Availability Statement: All relevant data are within the manuscript and its [Supporting Information](#) files.

Funding: Funded study: Funding by the Deutsche Forschungsgemeinschaft is gratefully acknowledged (F.L.: DFG LA 2804/12-1, DFG LA 2804/15-1; M.S.: DFG SA 4141/1-1; <https://www.dfg.de/>). The funders had no role in study design, data collection and analysis, decision to publish, or preparation of the manuscript.

Introduction

Diffusion-weighted imaging (DWI) has become an indispensable technique for the detection of focal liver lesions (FLLs) [1]. The presence or absence of FLL is a key parameter for choosing the subsequent treatment path in many tumor diseases, e.g. neuroendocrine tumors [2]. In liver DWI, as in virtually all other fields of clinical DWI, the diffusion encoding is based on variations of the pulsed gradient approach introduced by Stejskal and Tanner [3], which is for

Competing interests: I have read the journal's policy and the authors of this manuscript have the following competing interests: A.S. and T.B.: Employees of Siemens Healthcare GmbH. M.S.: Board membership with Siemens Healthcare GmbH. This does not alter our adherence to PLOS ONE policies on sharing data and materials.

Abbreviations: ADC, Apparent diffusion coefficient; DWI, diffusion-weighted imaging; EPI, echo planar imaging; FLL, focal liver lesion; FloCo, flow-compensated; GRAPPA, GeneRalized Autocalibrating Partial Parallel Acquisition; IVIM, intravoxel incoherent motion; RECIST, Response Evaluation Criteria in Solid Tumors; SNR, signal-to-noise ratio; TE, echo time; TR, repetition time.

good reason; no other gradient time profile can match its b-value efficiency [4, 5], at least if one compares versions optimized in this regard [6–9]. As a variation of this approach, twice-refocused diffusion encoding has found widespread application as a means for minimizing eddy current artifacts [10]. However, to our knowledge, no additional diffusion encodings have been widely applied in clinical MRI.

Nonetheless, a plethora of available diffusion encodings exist that exhibit fascinating properties, including oscillating gradients [11, 12], double diffusion encoding [13], and intensity-modulated two-gradient-pulse encoding [14], which all enable visualization of a range of microstructural tissue features, such as average cell surface-to-volume ratio [11] or even cell shape distribution (at least in certain limits) [14]. While extensively explored in a research context, it is presumably the high complexity of these advanced diffusion encodings, the need for extended scan time, and the rigorous technical demands that have so far prevented their transition into the broader clinical routine.

One specific diffusion encoding may stand out in this respect: flow-compensated (FloCo) diffusion encoding [15–20]. It suppresses the effect of signal decays induced by ballistic motion [15–18, 21] at the price of an increased minimally achievable echo time (TE) and a longer repetition time (TR). Overcoming these signal decays is relevant in several parts of the human body, but potentially nowhere to the same extent as in the left liver lobe due to its proximity to the heart [22, 23].

FloCo diffusion encoding can reduce the pulsation artifact considerably, as has been shown in a series of healthy volunteer investigations [6, 7, 24–26], although to our knowledge, until now, only one dataset from a single patient with FLLs has been presented [25]. In these patient images, a lesion was visible in the left liver lobe only with FloCo diffusion encoding. We are not aware of further studies clinically evaluating FloCo diffusion encodings for the detection of metastatic FLLs.

We hypothesized that a reduction in pulsation artifacts should lead to a more effective FLL detection in patients and conducted a prospective study to compare FloCo diffusion encoding to conventional monopolar diffusion encoding for the detection of liver metastases in oncologic patients.

Materials and methods

Study population

Patients aged ≥ 18 years were recruited prospectively from January to August 2020. To maximize the number of measured FLLs while minimizing the number of total scans, only patients who were known to have multiple malignant FLLs, or whose medical records made it likely that multiple malignant FLLs were present, were asked to participate in the study (stage IV cancer patients). Further inclusion criteria were a high probability that the patient would tolerate the examination prolonged by the study sequences, and written informed consent. Exclusion criteria were the presence of active or ferromagnetic implants, claustrophobia, tattoos close to the eyes, and sedative medications. All participants had a scheduled clinical MR examination and were recruited during the clinical workflow. The study was approved by the local Institutional Ethics Committee (study number, 276_19 B).

Magnetic resonance imaging

All measurements were performed on a clinical 1.5 T scanner (MAGNETOM Aera, XQ gradients with max. gradient strength 45 mT/m and max. slew rate 200 T/m/s, Siemens Healthcare, Erlangen, Germany) with an 18-channel anterior body coil in combination with a 32-channel spine array coil.

A vendor-provided prototype echo planar imaging (EPI) sequence was used featuring two diffusion encodings: Monopolar and FloCo. Monopolar is the vendor-specific name for the single-refocused diffusion encoding scheme. The vendor-provided sequence option ‘dynamic field correction’ was used to compensate for eddy current induced image distortions [10]. In the FloCo diffusion encoding used in this work, two pairs of monopolar gradients are placed symmetrically around the single 180° refocusing pulse of the spin-echo EPI sequence. Note that this placement strategy of the diffusion encoding gradients results in a nulled zeroth gradient moment during the 180° pulses and thus makes the use of crusher gradients necessary that are placed besides the 180° pulses even for b-values larger than zero. These crusher gradients are not flow-compensated (and neither is the EPI read-out) so that the flow-compensation is not perfect, strictly speaking. In the particular sequence implementation, the crusher gradients are merged with the diffusion encoding gradients. The TE of both DWI sequences was matched, to match the contrast-to-noise ratio (CNR). Table 1 summarizes the diffusion sequence parameters used to collect data before contrast agent administration.

Additionally, a standard clinical liver MRI protocol was performed for each patient, consisting of a T2-weighted HASTE sequence (repetition time [TR], 1000 ms; echo time [TE], 92 ms; slice thickness [ST], 5 mm); a fat-saturated T2-weighted TSE sequence (TR, 4848 ms; TE, 102 ms; ST, 5 mm); and fat-saturated T1-weighted GRE sequences (TR, 7.22 ms; TE, 2.39 ms; ST, 5 mm), one taken before and several after contrast agent administration (0.1 mmol/kg body weight; gadobutrol, Gadovist/Gadavist, Bayer Vital, Leverkusen, Germany). The contrast agent was administered after the diffusion sequences.

Table 1. MRI sequence parameters for FloCo and monopolar DWI sequences.

Sequence	DWI EPI
Repetition time (ms)	12,400
Echo time (ms)	70
Voxel size (mm ³)	3.125 × 3.125 × 5 interpolated to 1.6 × 1.6 × 5
Field of view (read × phase; mm ²)	400 × 325
Phase direction	anterior-posterior
Phase resolution	100%
Partial Fourier	6/8
Matrix	128 × 104
Slice distance	20%
Number of slices	39 (axial)
Parallel imaging	GRAPPA ×2, 24 reference lines
Bandwidth (Hz/pixel)	2,790
Echo spacing (ms)	0.49
b-values (s/mm ²)	50, 800
Averages (b50, b800)	1, 4
Diffusion mode	3-scan trace
Diffusion scheme	Once monopolar, once FloCo
Acquisition time (min:s)	3:43
Trigger	free breathing
Surface coil intensity correction	yes, the ‘pre-scan normalize’ option was used
Fat saturation	SPAIR & gradient reversal

DWI = diffusion-weighted imaging, EPI = echo planar imaging, GRAPPA = GeneRalized Autocalibrating Partial Parallel Acquisition, FloCo = flow-compensated, SPAIR = Spectral Adiabatic Inversion Recover

<https://doi.org/10.1371/journal.pone.0268843.t001>

Image analysis

After an initial quality check, the readers only assessed FLLs that they identified as metastases. Concomitant benign lesions (e.g., cysts, hemangiomas) were not scored. The readers used all available image data and the clinical radiology reports to differentiate the lesions.

Quantitative evaluation. The minimal and maximal lesion size was measured in the FloCo $b = 800 \text{ s/mm}^2$ (b800) images using the ruler tool according to the Response Evaluation Criteria in Solid Tumors (RECIST 1.1 [27]) criteria by a trained physicist (T.F.) under the supervision of a board-certified radiologist (S.B.). The diameters were measured only in the FloCo b800 images because the lesions were best visible there.

Under the supervision of two radiologists (M.S. and S.B.), a trained physicist (T.F., 2 years of experience in abdominal DWI) defined 3D segmentations with the Medical Imaging Interaction Toolkit (MITK, v2021.02, Heidelberg, Germany), encompassing the largest lesion in the left and right liver lobes for both diffusion encodings. The 3D volumes were defined with enough distance to the lesion borders to avoid partial-volume effects and used to calculate the apparent diffusion coefficient (ADC). As parallel imaging had been used, the standard deviation (SD) of the noise depended on the position and could not be assessed easily, e.g., using the SD of the signal in a region outside the body. Thus, following [28–31], the SD of the liver parenchyma in the specified ROI was used. It was estimated with an approximately 10 cm^2 2D segmentation drawn in a representative slice in the right liver lobe, sparing vessels. The signal-to-noise ratio (SNR) was then calculated by dividing the average signal in the 3D lesion segmentation by the standard deviation in the 2D liver segmentation.

The ADC was calculated from the signal averaged over the 3D lesion segmentations for three combinations (FloCo = b50-FloCo and b800-FloCo; Monopolar = b50-Monopolar and b800-Monopolar; Mixed = b50-Monopolar and b800-FloCo).

Qualitative whole-liver evaluation. Two board-certified radiologists (M.S. and H.S., 13 and 9 years of experience in abdominal imaging, respectively) independently rated the FloCo and monopolar datasets using 5-point Likert scales (1 = worst, 5 = best). The readers were not blinded to the acquisition type, as the distinction between the two techniques was obvious from the image impression.

To evaluate the image quality, the readers rated the following features (c.f. [31] for a detailed description of the scores):

- a. Overall image quality, once for b50 and once for b800, for both liver lobes combined (1 = very poor, 2 = poor, 3 = acceptable, 4 = good, 5 = very good), following [32–34].
- b. Blood signal blackness, once for b50 and once for b800, for both liver lobes combined (1 = very poor, 2 = poor, 3 = acceptable, 4 = good, 5 = very good).
- c. Severity of the cardiac motion artifact, once for the left and once for the right liver lobe, only for b800 as the artifact becomes only prominent at higher b-values (1 = liver lobe not identifiable, 2 = black holes frequently visible, 3 = strong signal loss and sporadic small black holes, 4 = slight signal loss, but no black holes, 5 = no signal loss visible), following [25].

Qualitative liver lesion evaluation. Following [31], the readers rated lesion conspicuity (Likert scale from 1 to 5) for small lesions ($< 1 \text{ cm}$) and large lesions ($\geq 1 \text{ cm}$) in each liver lobe. Lesion size was estimated visually and confirmed with the viewer's ruler tool, if necessary.

Lesion detection performance was evaluated separately for small and large lesions. As patients with known or expected presence of multiple FLLs were included in this study, the absolute number of detected lesions was not recorded. Instead, the readers counted the

number of lesions in the FloCo images and the monopolar images, and the difference in the number of lesions, expressed as Δ_{lesions} , was calculated by subtracting the number of monopolar lesions from the number of FloCo lesions. A positive value indicated that there were more lesions found with FloCo than with monopolar encoding, while a negative value indicated that more lesions were found with monopolar than with FloCo encoding. To simplify the evaluation, $\Delta_{\text{lesions}} \geq 3$ was set to $\Delta_{\text{lesions}} = 3$ and $\Delta_{\text{lesions}} \leq -3$ was set to $\Delta_{\text{lesions}} = -3$.

Statistical analysis

Statistical analysis was performed with MATLAB Release 2017b (The MathWorks, Inc., Natick, MA, USA). Significant differences in the absolute qualitative Likert scores between FloCo and monopolar diffusion encoding were tested using the non-parametric Wilcoxon signed-rank test. To assess the differences in SNR and ADC values between FloCo and

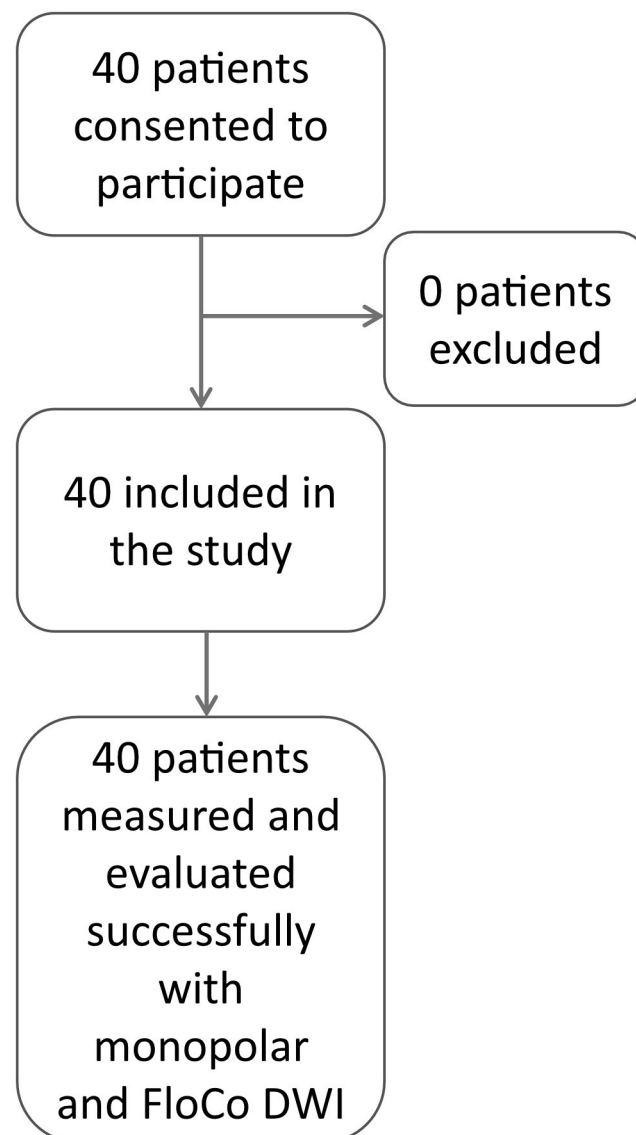


Fig 1. Participant flow diagram. Footnote: FloCo = Flow-compensated. DWI = diffusion-weighted imaging.

<https://doi.org/10.1371/journal.pone.0268843.g001>

monopolar diffusion encoding, the Shapiro–Wilk test was performed to test for normality. Subsequently, either a one-way ANOVA or a parametric test was performed (Wilcoxon signed-rank test or Kruskal–Wallis test). Additionally, post hoc tests were performed using Tukey’s honestly significant difference procedure. The inter-reader agreement was assessed by computing Cohen’s kappa (κ). A p-value < 0.05 was considered significant. The SNR, ADC, and smallest and largest visible lesions were described with descriptive statistics.

Results

Patients

Forty consecutive patients were enrolled in this study (27 males, 13 females). The mean participant age was 60 ± 9 years (range: 34–74 years). All liver MRI scans were successfully and completely performed and passed the initial quality check. Quantitative and qualitative evaluations were performed for all participants. FLLs were present in all participants. Fig 1 displays the participant inclusion flow diagram and Table 2 summarizes further participant demographics and disease characteristics.

Representative images

Figs 2–5 illustrate representative cases. In all four examples, lesions were reported in the FloCo datasets and were missed or much less visible in the monopolar datasets.

Quantitative image analysis

Table 3 and Fig 6 summarize the quantitative and test statistics for the SNR in the largest lesion present in the right and left liver lobes measured with monopolar and FloCo acquisition at b800. Furthermore, the results for ADC and the diameter of the smallest and largest visible lesions in the left and right liver lobes are given. Small lesions were regularly present. A significant difference was found between the lesion SNRs measured with the two diffusion encodings for both liver lobes (one-way ANOVA for the left liver lobe; Wilcoxon signed-rank test for right liver lobe used because of failed Shapiro–Wilk test). The mean, median, minimum, quartile 1, quartile 3, and maximum SNR in the left liver lobe lesions

Table 2. Patient demographics and disease characteristics.

Disease	Number of patients
Neuroendocrine tumor	21/40 (52.5%)
Colorectal cancer	10/40 (25.0%)
Thyroid cancer	4/40 (10.0%)
Melanoma	2/40 (5.0%)
Mixed adeno-neuroendocrine carcinoma	1/40 (2.5%)
Pancreatic cancer	1/40 (2.5%)
Non-small cell lung cancer	1/40 (2.5%)
No evaluation of right liver lobe due to hemihepatectomy	3
No evaluation of left liver lobe due to hemihepatectomy	1
At least one lesion < 1 cm present in right liver lobe	34
At least one lesion > 1 cm present in right liver lobe	31
At least one lesion < 1 cm present in left liver lobe	32
At least one lesion > 1 cm present in left liver lobe	30

The disease type was confirmed histologically, though not for each assessed lesion.

<https://doi.org/10.1371/journal.pone.0268843.t002>

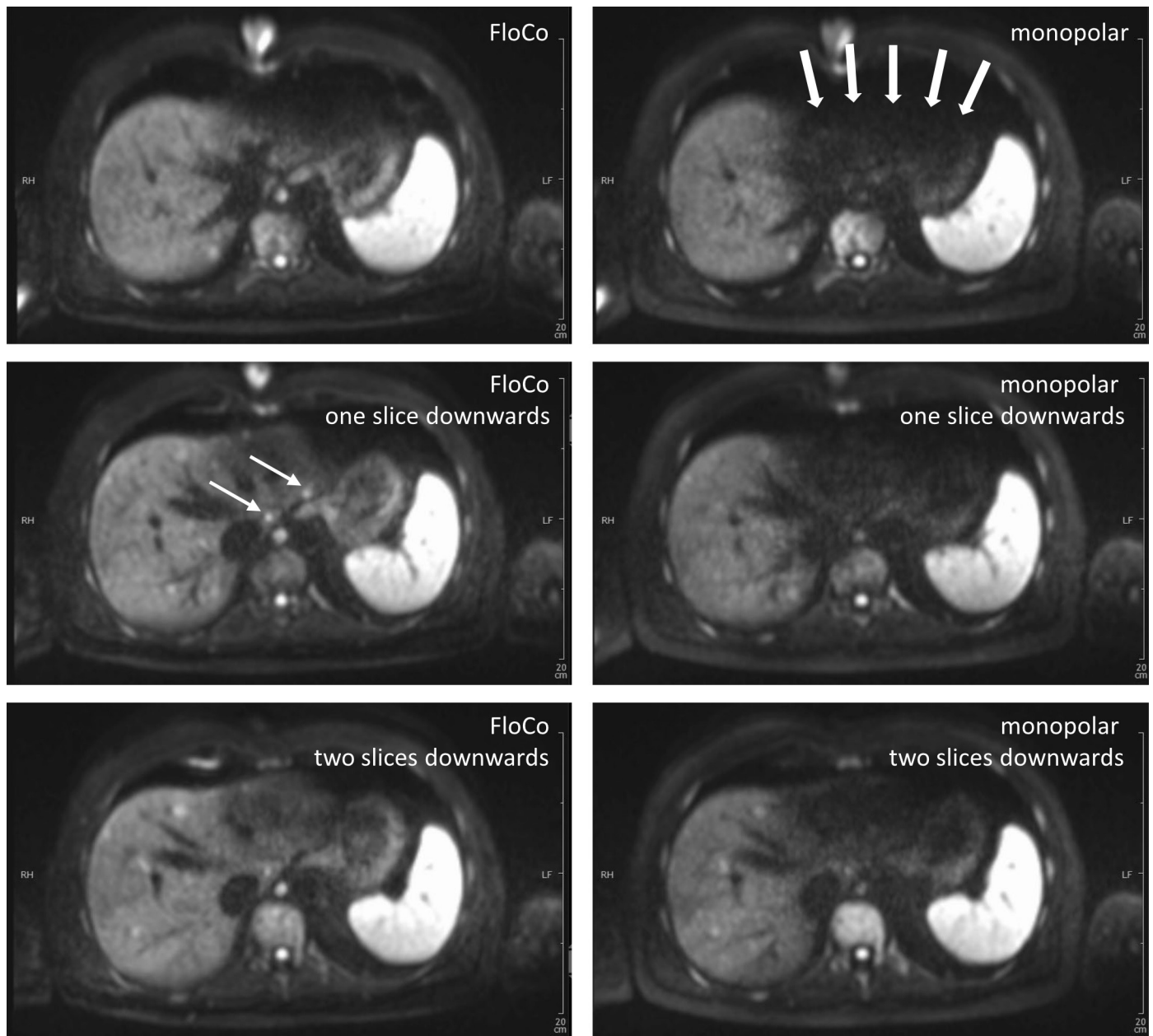


Fig 2. Diffusion-weighted b800 images of the liver in a 42-year-old patient with metastatic medullary thyroid carcinoma. Three adjacent slices, left-side flow-compensated (FloCo), right-side conventional monopolar diffusion encoding. There are considerable pulsation artifacts with monopolar diffusion encoding, which mask focal lesions in the left liver lobe (thick arrows). One of the arrow-marked small lesions was not reported by either of the two readers in the monopolar dataset. The other arrow-marked small lesion was not reported by one of the readers in the monopolar dataset.

<https://doi.org/10.1371/journal.pone.0268843.g002>

were approximately 30% higher with FloCo than with monopolar encoding. In the right liver lobe, the effect size was less, with approximately 10% to 15% increased SNR with FloCo than with monopolar encoding. The quantitative difference between the monopolar and FloCo ADCs was small, but the mixed ADC (calculated with b50-Monopolar and b800-FloCo) was reduced by approximately 15%. The differences between the three ADCs (Monopolar, FloCo, and Mixed) were significant (for the left and right liver lobe). The post hoc evaluation revealed no significant differences between monopolar and FloCo ADCs (in

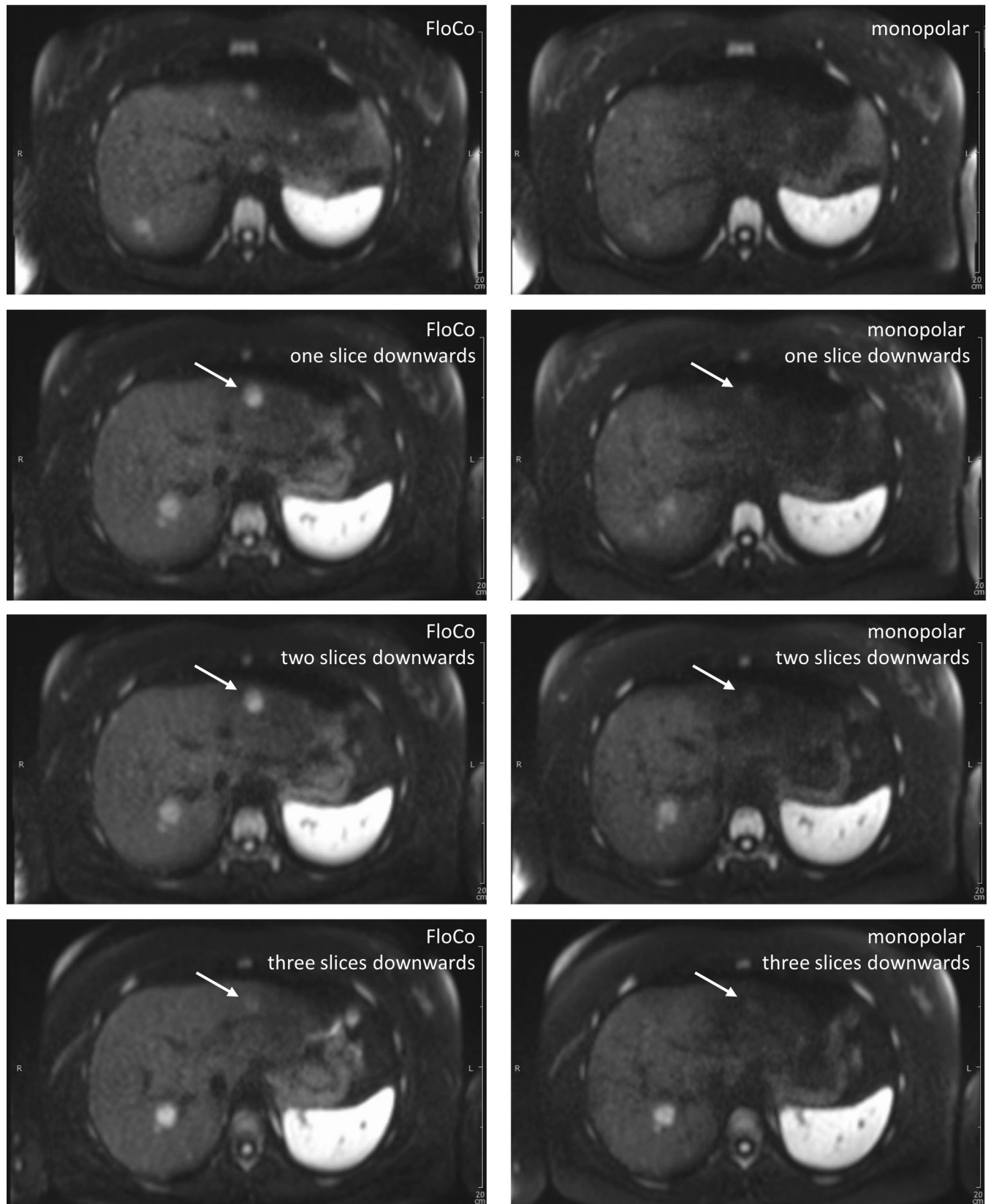


Fig 3. Diffusion-weighted b800 images of the liver in a 39-year-old patient with a metastatic neuroendocrine tumor of the jejunum. Four adjacent slices, left-side flow-compensated (FloCo), right-side monopolar diffusion encoding. The arrow-marked large lesion was detected by both readers but is much less visible in the monopolar dataset.

<https://doi.org/10.1371/journal.pone.0268843.g003>

left and right liver lobes), but a significant difference was found between FloCo and mixed ADC (for left and right liver lobes).

S1 Fig shows ADC maps computed with monopolar b50 data combined once with FloCo b800 data (i.e., mixed) and once with monopolar b800 data (i.e., monopolar) as well as ADC maps computed from FloCo data alone (i.e., FloCo). The mixed and monopolar maps are of similar quality, but the quality of the FloCo map is somewhat lower. This indicates that the proposed mixed-acquisition protocol (i.e., acquiring b50 monopolar and b800 FloCo data) may also yield ADC maps of sufficient quality.

An extended evaluation of the ADC maps was not performed because many ADC maps were corrupted by breathing motion (the influence of which is visible at the thick arrow). The use of navigator triggering might have mitigated this breathing-related problem but was not possible with the prototype sequence.

Qualitative image analysis

Fig 7 shows histograms of the Likert score evaluation for monopolar and FloCo diffusion encoding, with the pooled data of the two readers presented. Tables 4 and 5 show the individual reader data. The overall image quality was significantly better with the FloCo diffusion encoding at both b-values (for both readers). The black-blood state was reached significantly better at b50 with monopolar diffusion encoding (for both readers), but no significant difference was observed at b800 ($p \geq 0.25$ for both readers). In contrast, the pulsation artifact was significantly less with FloCo diffusion encoding at both b-values (for both readers).

No negative values were calculated for Δ_{lesions} , indicating that more or equal numbers of lesions were detected with FloCo diffusion encoding than with monopolar diffusion encoding for all participants. In the left liver lobe with FloCo diffusion encoding, readers 1 and 2 found six and seven additional small lesions, respectively, and one additional large FLL both. In the right liver lobe, readers 1 and 2 found five and seven additional small lesions, respectively, with FloCo diffusion encoding, and no additional large lesions.

Cohen's κ was ≥ 0.67 in all considered cases, indicating *substantial* or *almost perfect* agreement according to Landis and Koch [35].

Discussion

We evaluated the suitability of conventional monopolar and flow-compensated (FloCo) diffusion encoding for the detection of focal liver lesions in oncologic patients. With flow-compensated encoding, the pulsation artifact was reduced and more lesions were detected. Moreover, the overall image quality was superior and the blood was sufficiently dark at b800. Thus, flow-compensated encoding appears to be better suited for the detection of focal liver lesions.

Different techniques have been described to reduce pulsation artifacts in the liver. In this work we focused on a modified DWI sequence with FloCo diffusion encoding. Yet, there are alternative approaches, one of which is electrocardiogram (ECG) triggers [36, 37]. However, several drawbacks of ECG triggering impede its widespread use in clinical DWI. It is cumbersome to use the ECG trigger, and the rapid switching of diffusion gradient often degrades the ECG signal quality. Breathing navigator triggers have also been recommended, particularly for the detection of small FLLs [31]. However, using ECG and breathing triggers simultaneously would presumably extend the scan time to an unacceptable degree.

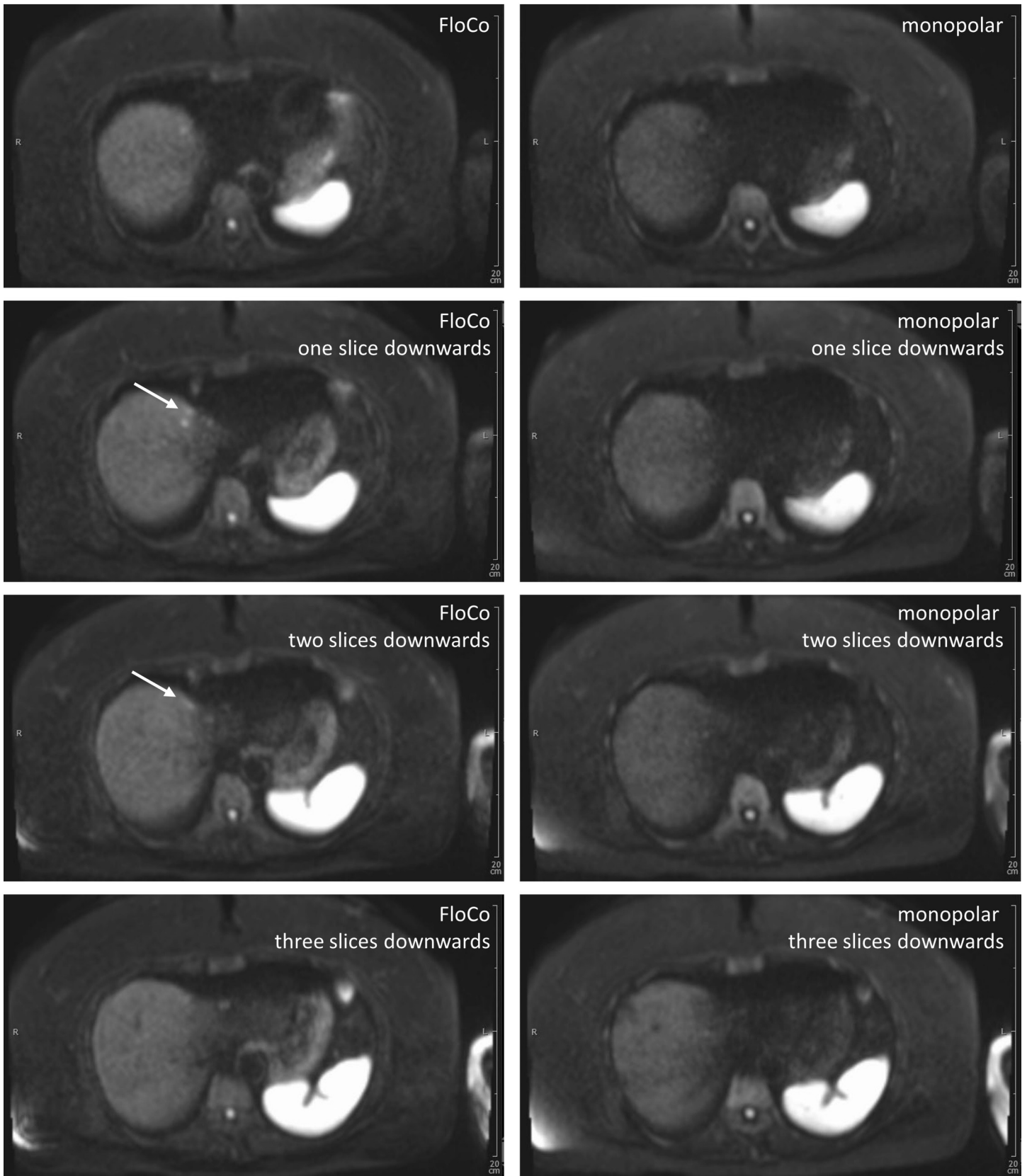


Fig 4. Diffusion-weighted b800 images of the liver in a 61-year-old patient with a metastatic neuroendocrine tumor of the ileum. Four adjacent slices, left-side flow-compensated (FloCo), right-side monopolar diffusion encoding. The arrow-marked small lesion was not reported by either of the two readers in the monopolar dataset. The adjacent lesion is barely visible in the monopolar dataset.

<https://doi.org/10.1371/journal.pone.0268843.g004>

The pulsation artifact can also be reduced with postprocessing techniques. Ichikawa et al. and Liau et al. proposed two approaches involving averaging multiple acquired images such that stronger signal intensities are more heavily weighted [38, 39]. This reduces the signal void, a characteristic of the pulsation artifact, in the averaged images. Similar methods could be applied to FloCo diffusion encoding data, but a straightforward application might be difficult to achieve. For example, the blood signal was sufficiently dark at b800 in the averaged images investigated in our study, but this is not necessarily true for each acquired FloCo image, unlike for the monopolar images [25]. The described weighted average approaches could then lead to a bright blood signal at some image positions. Thus, we did not use advanced postprocessing approaches in our current study, although we deem it likely that they could lead to further improvements if carefully adapted.

At b50, the black-blood property received mostly high ratings (i.e., Likert scores of 4 and 5, c.f. Fig 7) for both diffusion encoding methods, though monopolar generally performed better. At b800, this difference virtually disappeared. This is consistent with Rauh et al.'s [25] proposal to use monopolar diffusion encoding for b50 images and FloCo diffusion encoding for b800 images. ADC maps might then be computed from b50-Monopolar and b800-FloCo data (S1 Fig). In our setup, images acquired with two consecutively run sequences were combined for this purpose. As readjustments between the sequences may potentially alter image intensities, a more favorable approach in future implementations would be to acquire all data within one sequence thus avoiding potentially occurring biases due to readjustments between the sequences. An alternative approach to suppress the blood signal at low b-values is to use partially flow-compensated diffusion encoding [26, 40].

The finding that the SNR was increased with FloCo diffusion encoding may be interpreted as a reduction of the pulsation artifact. But this interpretation is limited in so far as the signal decay due to the IVIM effect is also reduced for FloCo diffusion encoding. [18].

Concerning the ADC, the different temporal spectrum of the monopolar and FloCo diffusion encoding [11, 12, 41] might have some influence altering the ADC, although we believe that the quantitative impact on the ADC should be small, i.e. on the order of below 10%, given the similar slopes of the signal decay curves observed by Wetscherek et al. in the liver for monopolar and FloCo diffusion encoding [18]. The occurrence of the smaller ADC values observed for the mixed approach can be well explained by the IVIM model in the ballistic limit [17]. The monopolar signal at b50 experiences the IVIM-related signal drop, but the FloCo signal at b800 does not (in the ballistic limit). Hence, the signal drops less from b50 to b800 compared to the “not mixed” approach—and the ensuing ADC is decreased.

We used the minimal TE achievable with the FloCo sequence at b800 both for FloCo and monopolar diffusion encoding (i.e., TE = 70 ms, TE = 46 ms would have been possible with monopolar diffusion encoding). The TE of 70 ms lies within the values used in other patient studies, which range from 49.7 ms to 82 ms at 1.5 T [42–46]. Although Taouli and Koh [47] suggested in their review to use the minimal achievable TE, which they found to be approximately 71 ms with their system, it seems reasonable to maximize the CNR. Assuming that the proton density and the noise are identical in liver and lesion, the respective optimal TE is achieved when the contrast between liver and lesion becomes maximal, i.e. at

$$TE_{\text{opt}} = \frac{1}{T_{2,\text{liver}}^{-1} - T_{2,\text{lesion}}^{-1}} \log \frac{T_{2,\text{lesion}}}{T_{2,\text{liver}}},$$

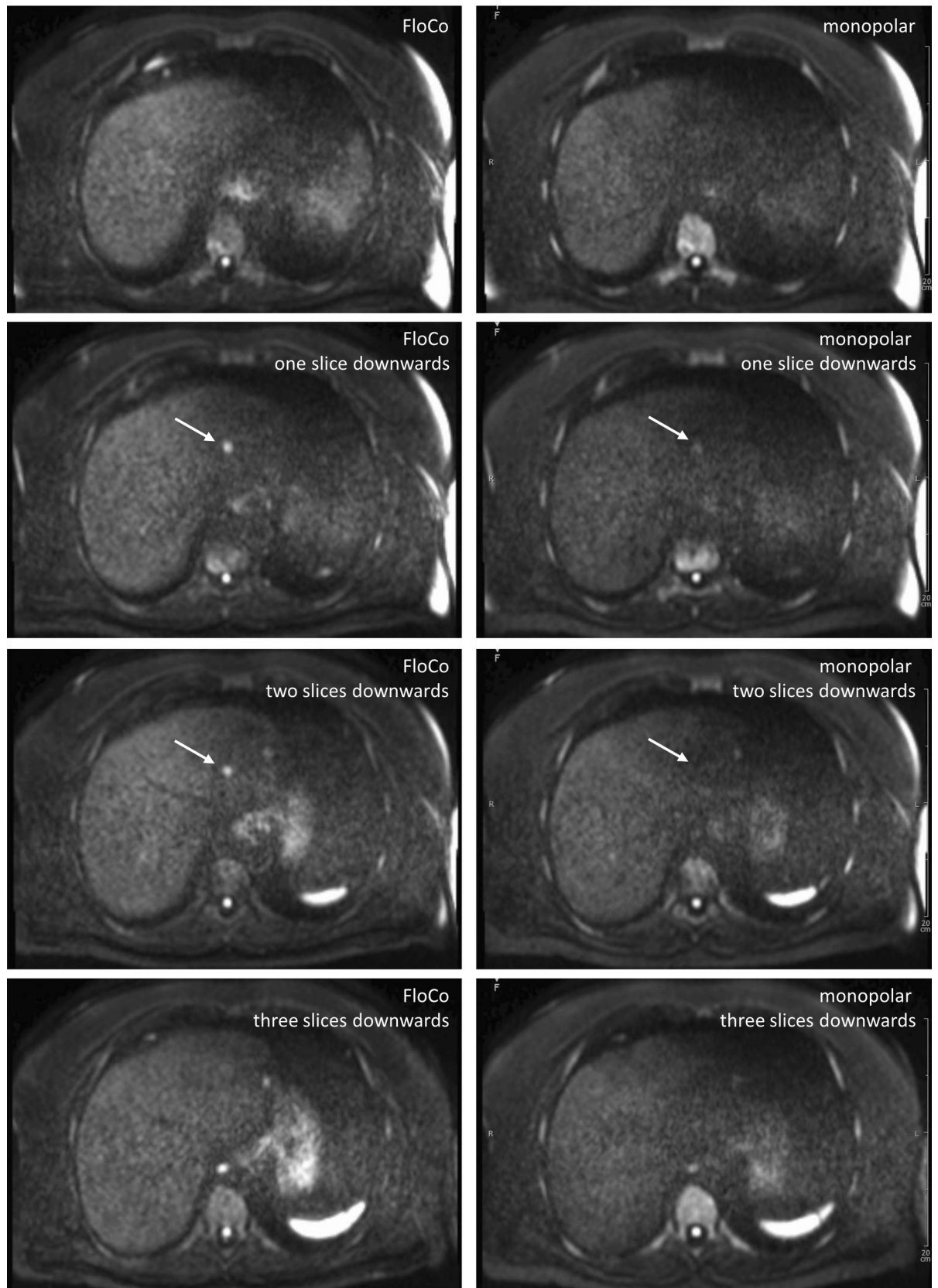


Fig 5. Diffusion-weighted b800 images of the liver in a 70-year-old patient with a metastatic neuroendocrine tumor of unknown primary. Four adjacent slices, left-side flow-compensated (FloCo), right-side monopolar diffusion encoding. The conspicuity was rated higher for the FloCo data by both readers (with a Likert score of 2).

<https://doi.org/10.1371/journal.pone.0268843.g005>

with the transversal relaxation times $T_{2,liver}$ and $T_{2,lesion}$ of liver tissue and lesion, respectively. For example, Cieszanowski et al. reported $T_{2,liver} = 54$ ms and $T_{2,lesion} = 85$ ms at 1.5 T. Consequently, $TE_{opt} \approx 67$ ms, which is very close to the setting that we had used ($TE = 70$ ms). Thus, the fact that the minimally achievable echo time is prolonged with the FloCo diffusion encoding is presumably not a decisive disadvantage in clinical practice.

The difference in found lesions, $\Delta_{lesions}$, was rated significantly different between the two acquisition schemes by reader 1 for small lesions in the right liver lobe (but not by reader 2). Both readers did not find a significant difference for the left liver lobe. This is somewhat astonishing, since the left liver lobe is more prone to the pulsation artifact, but may be explained by the smaller size of the left liver lobe and the therewith reduced total number of lesions. The p-value was indeed only slightly above the significance threshold ($p = 0.063$) for the left liver lobe. Thus, although not significant, the probability that this result occurred by chance is only 6.3% (with the null hypothesis that no effect was present).

This study has several limitations. First, the acquisition was performed in the free-breathing mode because the prototype sequence did not allow for breathing navigator triggering. Particularly for smaller lesions, the use of breathing navigator triggering would presumably have been advantageous [31]. However, both DWI sequences were scanned in free breathing allowing for a fair comparison. Second, the TR was relatively long due to FloCo diffusion encoding posing high demands on the gradient system cooling rate. This drawback will likely become less severe as new generations of high-performance gradient systems are developed. Third, only one scanner from one vendor at one site was used in this study, potentially reducing the generalizability of the obtained results. Yet, we used a widespread

Table 3. Descriptive statistics of the quantitative lesion evaluation.

	Liver lobe	Diffusion encoding	Mean ± Standard deviation	Minimum	Median [Q1 Q3]	Maximum	p-value (Shapiro-Wilk)	p-value (Mp vs FC)	p-value (post hoc test) (ADC: Mp vs FC, Mp vs mixed, FC vs mixed)
Lesion SNR (b800)	Left	Monopolar	15.24 ± 6.84	3.56	13.83 [10.17 20.01]	33.07	0.61	0.007	
		FloCo	20.20 ± 7.47	6.22	20.17 [16.56 25.85]	37.16	0.67		
	Right	Monopolar	19.62 ± 7.96	7.13	19.60 [13.32 24.12]	48.37	< 0.01	< 0.001	
		FloCo	23.46 ± 9.02	9.74	23.19 [16.68 28.39]	47.26	0.047		
Lesion ADC ($\mu\text{m}^2/\text{ms}$)	Left	Monopolar	1.52 ± 0.61	0.81	1.34 [1.08 1.69]	3.53	< 0.001	0.0175	Mp/FC: 0.97 Mp/mixed: 0.028 FC/mixed: 0.0499
		FloCo	1.45 ± 0.51	0.85	1.33 [1.14 1.47]	3.27	< 0.001		
		Mixed	1.24 ± 0.45	0.68	1.12 [0.96 1.33]	2.81	< 0.001		
	Right	Monopolar	1.16 ± 0.40	0.21	1.19 [0.92 1.34]	2.56	0.02	0.0159	
		FloCo	1.20 ± 0.31	0.71	1.13 [1.00 1.34]	2.48	< 0.001		
		Mixed	1.03 ± 0.35	0.34	0.96 [0.84 1.09]	2.41	< 0.001		
Diameter (smallest lesion; mm)	Left	FloCo	6.99 ± 3.87	3.88	5.86 [5.05 6.99]	20.37			
	Right		8.15 ± 7.31	3.72	5.68 [4.94 7.57]	40.02			
Diameter (largest lesion; mm)	Left	32.47 ± 24.19	4.65	25.01 [15.22 42.70]	102.65				
	Right	35.54 ± 29.38	3.95	26.12 [13.48 52.63]	118.78				

Significant p-values are in bold font. Mixed ADC was calculated with b50 monopolar and b800 FloCo data. The parametric test was the Wilcoxon signed-rank test for the SNR and the Kruskal-Wallis test for the ADC. Q1 = Quartile 1, Q3 = Quartile 3. FC = FloCo = Flow-compensated. Mp = monopolar.

<https://doi.org/10.1371/journal.pone.0268843.t003>

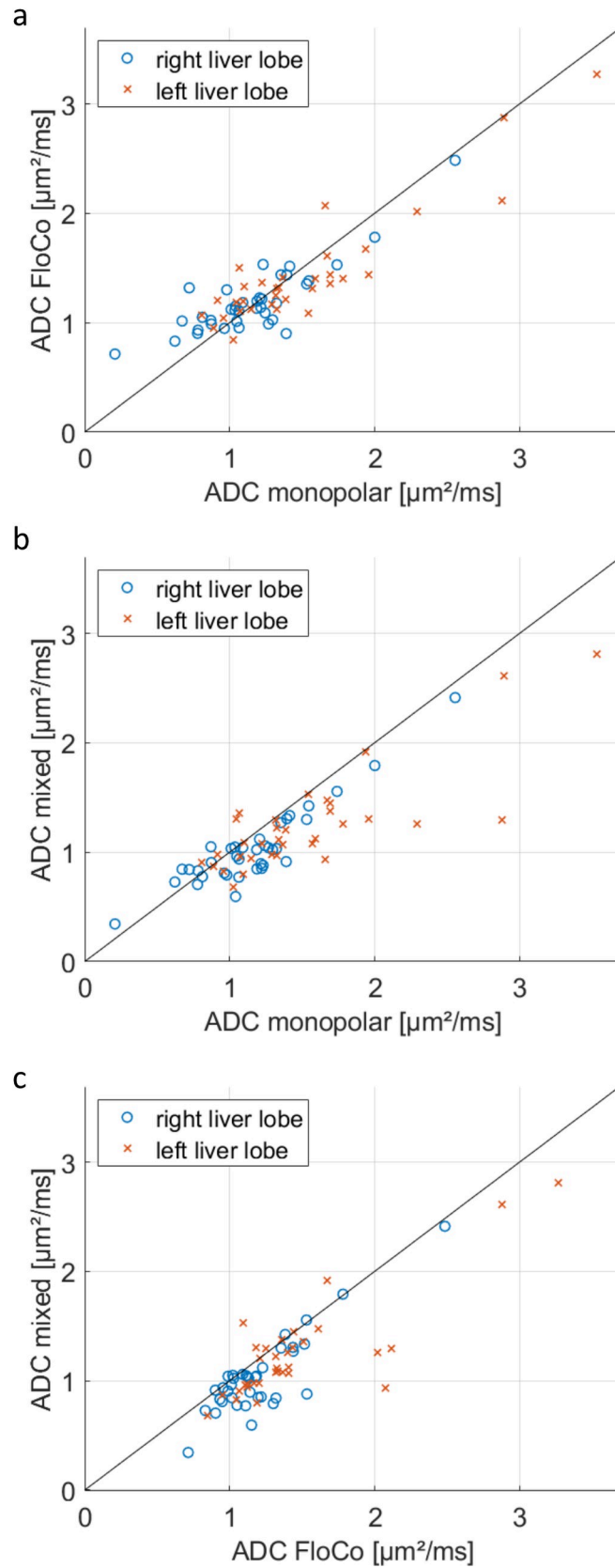


Fig 6. Individual subject ADC values for monopolar, FloCo, and mixed diffusion schemes.

<https://doi.org/10.1371/journal.pone.0268843.g006>

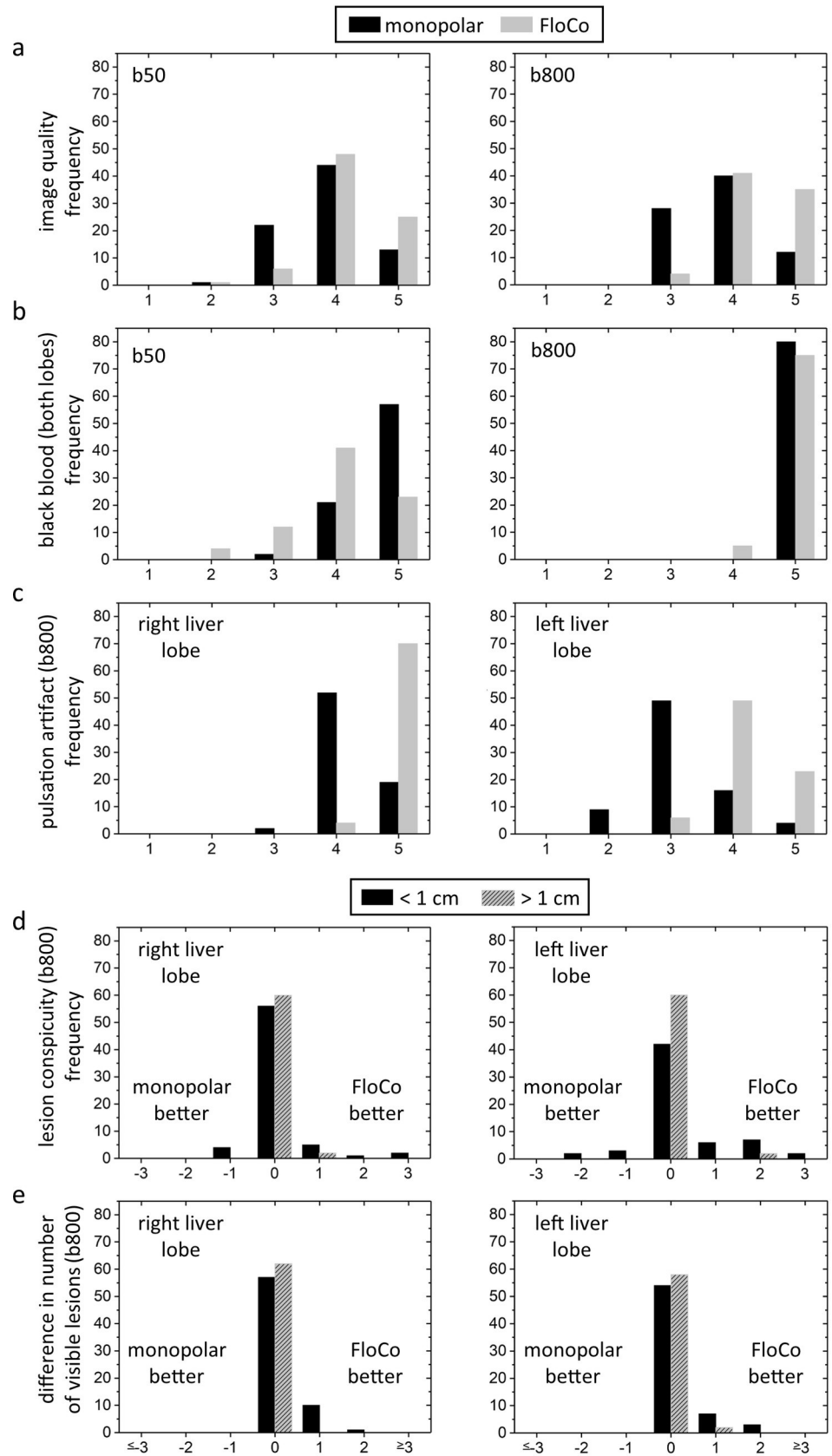


Fig 7. Histograms of the qualitative lesion evaluation. The scales in a) to d) range from 1 (worst) to 5 (best). Difference in number of visible lesions (Δ_{lesions}) is plotted in e) and calculated as number of lesions visible with flow-compensated (FloCo) minus number of lesions visible with monopolar diffusion encoding. A positive score indicates that more lesions were found with FloCo diffusion encoding.

<https://doi.org/10.1371/journal.pone.0268843.g007>

1.5 T MRI scanner from a large vendor. Finally, the malignancy of the lesions was not confirmed histologically for all lesions, causing us to rely on radiological classification. However, the read was performed by board-certified radiologists with extensive clinical experience in classification of liver lesions. The remaining uncertainty on the true lesion status should not be a major limitation of our study, which was focused on lesion conspicuity rather than on differentiating lesion types.

Conclusions

In conclusion, the use of liver diffusion-weighted imaging with flow-compensated diffusion encoding is feasible on a currently widespread clinical 1.5 T MR scanner. The previously observed reduction in pulsation artifacts with flow-compensated diffusion encoding in healthy young volunteers was reproduced in older patients with focal liver lesions. We found that artifact reduction supported the detection of focal liver lesions compared to the conventional monopolar diffusion encoding by increasing the number of visible lesions.

Table 4. Qualitative Likert score evaluation by reader 1 and reader 2 (same data as in Fig 7).

	Liver lobe	b-value	Diffusion encoding	Reader	1	2	3	4	5	p-value R1	p-value R2	κ
Image quality	Left & right	b50	Monopolar	R1	0	1	12	20	7	0.008	0.001	0.62
				R2	0	0	10	24	6			
			FloCo	R1	0	1	3	25	11			0.49
				R2	0	0	3	23	14			
	Left & right	b800	Monopolar	R1	0	0	14	19	7	< 0.001	< 0.001	0.51
				R2	0	0	14	21	5			
			FloCo	R1	0	0	3	19	18			0.68
				R2	0	0	1	22	17			
Black-blood signal	Left & right	b50	Monopolar	R1	0	0	2	9	29	< 0.001	< 0.001	0.82
				R2	0	0	0	12	28			
			FloCo	R1	0	3	6	19	12			0.72
				R2	0	1	6	22	11			
	Left & right	b800	Monopolar	R1	0	0	0	0	40	.50	.25	1.00
				R2	0	0	0	0	40			
			FloCo	R1	0	0	0	2	38			0.79
				R2	0	0	0	3	37			
Pulsation artifact	Left	b800	Monopolar	R1	0	5	25	7	2	< 0.001	< 0.001	0.67
				R2	0	4	24	9	2			
			FloCo	R1	0	0	4	24	11			0.75
				R2	0	0	2	25	12			
	Right	b800	Monopolar	R1	0	0	1	28	8	< 0.001	< 0.001	0.81
				R2	0	0	1	25	11			
			FloCo	R1	0	0	0	2	35			1.00
				R2	0	0	0	2	35			

Significant p-values are printed in bold font.

<https://doi.org/10.1371/journal.pone.0268843.t004>

Table 5. Lesion conspicuity and the difference in detectable lesions (Δ_{lesions}) (same data as in Fig 7).

	Liver lobe	b-value	Diffusion encoding	Lesion size	Reader	-3	-2	-1	0	1	2	3	p-value	κ		
Lesion conspicuity	Left	b800	FloCo vs monopolar	Small	R1	0	1	1	22	3	4	1	0.078	0.81		
					R2	0	1	2	22	3	3	1	0.197			
			FloCo vs monopolar	Large	R1	0	0	0	29	0	1	0	1.000	1.00		
					R2	0	0	0	29	0	1	0	1.000			
	Right	b800	FloCo vs monopolar	Small	R1	0	0	2	28	2	1	1	0.375	0.91		
					R2	0	0	2	28	3	0	1	0.531			
			FloCo vs monopolar	Large	R1	0	0	0	30	1	0	0	1.000	1.00		
					R2	0	0	0	30	1	0	0	1.000			
Δ_{lesions}	Left	b800	FloCo vs monopolar	Small	R1	0	0	0	27	4	1	0	0.063	0.89		
					R2	0	0	0	27	3	2	0	0.063			
			FloCo vs monopolar	Large	R1	0	0	0	29	1	0	0	1.000	1.00		
					R2	0	0	0	29	1	0	0	1.000			
			Right	b800	FloCo vs monopolar	Small	R1	0	0	0	29	5	0	0	0.063	0.79
							R2	0	0	0	28	5	1	0	0.031	
	FloCo vs monopolar	Large			R1	0	0	0	31	0	0	0	1.000	1.00		
					R2	0	0	0	31	0	0	0	1.000			

Significant p-values are printed in bold font. Lesion conspicuity: scores larger than zero indicate lesions that were better visible with FloCo encoding. Δ_{lesions} : values larger than zero indicate that more lesions were detectable with FloCo encoding.

<https://doi.org/10.1371/journal.pone.0268843.t005>

Supporting information

S1 Fig. ADC maps computed with monopolar b50 data combined once with FloCo b800 data (i.e., mixed) and once with monopolar b800 data (i.e., monopolar) as well as ADC maps computed from FloCo data alone (i.e., FloCo).
(TIF)

S1 Table. Minimal data set of this study.
(XLSX)

Author Contributions

Conceptualization: Frederik B. Laun, Alto Stemmer, Michael Uder, Marc Saake.

Data curation: Tobit Führes, Marc Saake.

Formal analysis: Frederik B. Laun, Hannes Seuss, Astrid Müller, Sebastian Bickelhaupt, Marc Saake.

Funding acquisition: Frederik B. Laun, Marc Saake.

Investigation: Frederik B. Laun, Tobit Führes, Hannes Seuss, Astrid Müller, Sebastian Bickelhaupt, Marc Saake.

Methodology: Frederik B. Laun, Astrid Müller, Alto Stemmer, Thomas Benkert.

Software: Frederik B. Laun, Tobit Führes, Astrid Müller.

Supervision: Frederik B. Laun, Sebastian Bickelhaupt, Michael Uder, Marc Saake.

Validation: Frederik B. Laun, Tobit Führes, Astrid Müller, Sebastian Bickelhaupt, Marc Saake.

Visualization: Frederik B. Laun.

Writing – original draft: Frederik B. Laun.

Writing – review & editing: Tobit Führes, Hannes Seuss, Astrid Müller, Sebastian Bickelhaupt, Alto Stemmer, Thomas Benkert, Michael Uder, Marc Saake.

References

1. Donato H, Franca M, Candelaria I, Caseiro-Alves F. Liver MRI: From basic protocol to advanced techniques. *Eur J Radiol.* 2017; 93:30–9. Epub 2017/07/03. <https://doi.org/10.1016/j.ejrad.2017.05.028> PMID: 28668428.
2. Cives M, Strosberg JR. Gastroenteropancreatic Neuroendocrine Tumors. *Ca-Cancer J Clin.* 2018; 68(6):471–87. <https://doi.org/10.3322/caac.21493> PubMed PMID: WOS:000450033500006. PMID: 30295930
3. Stejskal EO, Tanner JE. Spin Diffusion Measurements: Spin Echoes in the Presence of a Time-Dependent Field Gradient. *The Journal of Chemical Physics.* 1965; 42:288.
4. Grebenkov DS. NMR survey of reflected Brownian motion. *Rev Mod Phys.* 2007; 79(3):1077–137. <https://doi.org/10.1103/RevModPhys.79.1077> PubMed PMID: WOS:000248867000009.
5. Laun FB, Kuder TA, Zong FR, Hertel S, Galvosas P. Symmetry of the gradient profile as second experimental dimension in the short-time expansion of the apparent diffusion coefficient as measured with NMR diffusometry. *J Magn Reson.* 2015; 259:10–9. <https://doi.org/10.1016/j.jmr.2015.07.003> PubMed PMID: WOS:000363358800002. PMID: 26254733
6. Aliotta E, Wu HH, Ennis DB. Convex optimized diffusion encoding (CODE) gradient waveforms for minimum echo time and bulk motion-compensated diffusion-weighted MRI. *Magn Reson Med.* 2017; 77(2):717–29. <https://doi.org/10.1002/mrm.26166> PubMed PMID: WOS:000394544700028. PMID: 26900872
7. Pena-Nogales O, Zhang YX, Wang XK, de Luis-Garcia R, Aja-Fernandez S, Holmes JH, et al. Optimized Diffusion-Weighting Gradient Waveform Design (ODGD) formulation for motion compensation and concomitant gradient nulling. *Magn Reson Med.* 2019; 81(2):989–1003. <https://doi.org/10.1002/mrm.27462> PubMed PMID: WOS:000462086300022. PMID: 30394568
8. Aliotta E, Moulin K, Ennis DB. Eddy current-nulled convex optimized diffusion encoding (EN-CODE) for distortion-free diffusion tensor imaging with short echo times. *Magn Reson Med.* 2018; 79(2):663–72. <https://doi.org/10.1002/mrm.26709> PubMed PMID: WOS:000419134600006. PMID: 28444802
9. Middione MJ, Loecher M, Moulin K, Ennis DB. Optimization methods for magnetic resonance imaging gradient waveform design. *NMR in biomedicine.* 2020; 33(12). doi: ARTN e4308 <https://doi.org/10.1002/nbm.4308>. PubMed PMID: WOS:000528838900001.
10. Reese TG, Heid O, Weisskoff RM, Wedeen VJ. Reduction of eddy-current-induced distortion in diffusion MRI using a twice-refocused spin echo. *Magn Reson Med.* 2003; 49(1):177–82. <https://doi.org/10.1002/mrm.10308> PubMed PMID: WOS:000180148100023. PMID: 12509835
11. Reynaud O, Winters KV, Hoang DM, Wadghiri YZ, Novikov DS, Kim SG. Surface-to-Volume Ratio Mapping of Tumor Microstructure Using Oscillating Gradient Diffusion Weighted Imaging. *Magn Reson Med.* 2016; 76(1):237–47. <https://doi.org/10.1002/mrm.25865> PubMed PMID: WOS:000384996900024. PMID: 26207354
12. Stepisnik J. Analysis of NMR Self-Diffusion Measurements by a Density Matrix Calculation. *Physica B.* 1981; 104:350–64.
13. Shemesh N, Jespersen SN, Alexander DC, Cohen Y, Drobnjak I, Dyrby TB, et al. Conventions and Nomenclature for Double Diffusion Encoding NMR and MRI. *Magn Reson Med.* 2016; 75(1):82–7. <https://doi.org/10.1002/mrm.25901> PubMed PMID: WOS:000367739200008. PMID: 26418050
14. Laun FB, Kuder TA, Semmler W, Stieltjes B. Determination of the Defining Boundary in Nuclear Magnetic Resonance Diffusion Experiments. *Phys Rev Lett.* 2011; 107(4). doi: ARTN 048102 <https://doi.org/10.1103/PhysRevLett.107.048102> PubMed PMID: WOS:000292969100011. PMID: 21867047
15. Maki JH, MacFall JR, Johnson GA. The use of gradient flow compensation to separate diffusion and microcirculatory flow in MRI. *Magn Reson Med.* 1991; 17(1):95–107. <https://doi.org/10.1002/mrm.1910170114> PMID: 1712421.
16. Fujita N, Harada K, Sakurai K, Akai Y, Kozuka T. Separation of Diffusion and Slow Flow Effects by Use of Flow Rephasing and Dephasing. *Magnetic Resonance in Medicine.* 1992; 24(1):109–22. <https://doi.org/10.1002/mrm.1910240112> PubMed PMID: WOS:A1992HH85700011. PMID: 1556918
17. Ahlgren A, Knutsson L, Wirestam R, Nilsson M, Stahlberg F, Topgaard D, et al. Quantification of microcirculatory parameters by joint analysis of flow-compensated and non-flow-compensated intravoxel

- incoherent motion (IVIM) data. *NMR in biomedicine*. 2016; 29(5):640–9. <https://doi.org/10.1002/nbm.3505> PMID: 26952166; PubMed Central PMCID: PMC5069652.
18. Wetscherek A, Stieltjes B, Laun FB. Flow-compensated intravoxel incoherent motion diffusion imaging. *Magn Reson Med*. 2015; 74(2):410–9. <https://doi.org/10.1002/mrm.25410> PMID: 25116325.
 19. Brockstedt S, Thomsen C, Wirestam R, Depoorter J, Dewagter C, Salford LG, et al. Use of an Enhanced Gradient System for Diffusion Mr-Imaging with Motion-Artifact Reduction. *Acta Radiol*. 1995; 36(6):662–70. PubMed PMID: WOS:A1995TJ87900018. PMID: 8519581
 20. McTavish S, Van AT, Peeters JM, Weiss K, Makowski MR, Braren RF, et al. Gradient nonlinearity correction in liver DWI using motion-compensated diffusion encoding waveforms. *Magnetic Resonance Materials in Physics, Biology and Medicine*. 2021; <https://doi.org/10.1007/s10334-021-00981-6> PMID: 34894335
 21. Szczepankiewicz F, Sjolund J, Dall'Armellina E, Plein S, Schneider JE, Teh I, et al. Motion-compensated gradient waveforms for tensor-valued diffusion encoding by constrained numerical optimization. *Magn Reson Med*. 2021; 85(4):2117–26. <https://doi.org/10.1002/mrm.28551> PubMed PMID: WOS:000578743000001. PMID: 33048401
 22. Kwee TC, Takahara T, Niwa T, Ivancevic MK, Herigault G, Van Cauteren M, et al. Influence of cardiac motion on diffusion-weighted magnetic resonance imaging of the liver. *MAGMA*. 2009; 22(5):319–25. Epub 2009/09/04. <https://doi.org/10.1007/s10334-009-0183-1> PMID: 19727877.
 23. Riexinger A, Laun FB, Bickelhaupt S, Seuss H, Uder M, Hensel B, et al. On the dependence of the cardiac motion artifact on the breathing cycle in liver diffusion-weighted imaging. *PLoS One*. 2020; 15(10): e0239743. Epub 2020/10/02. <https://doi.org/10.1371/journal.pone.0239743> PMID: 33002028; PubMed Central PMCID: PMC7529231.
 24. Ozaki M, Inoue Y, Miyati T, Hata H, Mizukami S, Komi S, et al. Motion artifact reduction of diffusion-weighted MRI of the liver: use of velocity-compensated diffusion gradients combined with tetrahedral gradients. *J Magn Reson Imaging*. 2013; 37(1):172–8. <https://doi.org/10.1002/jmri.23796> PMID: 22987784.
 25. Rauh SS, Riexinger AJ, Ohlmeyer S, Hammon M, Saake M, Stemmer A, et al. A mixed waveform protocol for reduction of the cardiac motion artifact in black-blood diffusion-weighted imaging of the liver. *Magnetic Resonance Imaging*. 2020; 67:59–68. <https://doi.org/10.1016/j.mri.2019.12.011> PMID: 31923466.
 26. Zhang YX, Pena-Nogales O, Holmes JH, Hernando D. Motion-robust and blood-suppressed M1-optimized diffusion MR imaging of the liver. *Magn Reson Med*. 2019; 82(1):302–11. <https://doi.org/10.1002/mrm.27735> PubMed PMID: WOS:000481978800022. PMID: 30859628
 27. Eisenhauer EA, Therasse P, Bogaerts J, Schwartz LH, Sargent D, Ford R, et al. New response evaluation criteria in solid tumours: Revised RECIST guideline (version 1.1). *European Journal of Cancer*. 2009; 45(2):228–47. <https://doi.org/10.1016/j.ejca.2008.10.026> PubMed PMID: WOS:000262948300002. PMID: 19097774
 28. Kandpal H, Sharma R, Madhusudhan KS, Kapoor KS. Respiratory-triggered versus breath-hold diffusion-weighted MRI of liver lesions: comparison of image quality and apparent diffusion coefficient values. *AJR Am J Roentgenol*. 2009; 192(4):915–22. Epub 2009/03/24. <https://doi.org/10.2214/AJR.08.1260> PMID: 19304695.
 29. Choi JS, Kim MJ, Chung YE, Kim KA, Choi JY, Lim JS, et al. Comparison of breathhold, navigator-triggered, and free-breathing diffusion-weighted MRI for focal hepatic lesions. *Journal of Magnetic Resonance Imaging*. 2013; 38(1):109–18. <https://doi.org/10.1002/jmri.23949> PubMed PMID: WOS:000321614600013. PMID: 23188562
 30. Furuta A, Isoda H, Yamashita R, Ohno T, Kawahara S, Shimizu H, et al. Comparison of monopolar and bipolar diffusion weighted imaging sequences for detection of small hepatic metastases. *Eur J Radiol*. 2014; 83(9):1626–30. Epub 2014/07/07. <https://doi.org/10.1016/j.ejrad.2014.06.003> PMID: 24998079.
 31. Saake M, Seuss H, Riexinger A, Bickelhaupt S, Hammon M, Uder M, et al. Image Quality and Detection of Small Focal Liver Lesions in Diffusion-Weighted Imaging: Comparison of Navigator Tracking and Free-Breathing Acquisition. *Invest Radiol*. 2021; 56(9):579–90. Epub 2021/04/05. <https://doi.org/10.1097/RLI.0000000000000776> PMID: 33813572.
 32. Taouli B, Sandberg A, Stemmer A, Parikh T, Wong S, Xu J, et al. Diffusion-Weighted Imaging of the Liver: Comparison of Navigator Triggered and Breathhold Acquisitions. *Journal of Magnetic Resonance Imaging*. 2009; 30(3):561–8. <https://doi.org/10.1002/jmri.21876> PubMed PMID: WOS:000269472600013. PMID: 19711402
 33. Tavakoli A, Attenberger UI, Budjan J, Stemmer A, Nickel D, Kannengiesser S, et al. Improved Liver Diffusion-Weighted Imaging at 3 T Using Respiratory Triggering in Combination With Simultaneous Multi-slice Acceleration. *Invest Radiol*. 2019; 54(12):744–51. <https://doi.org/10.1097/RLI.0000000000000594> PubMed PMID: WOS:000497657600002. PMID: 31335634

34. Dreher C, Kuder TA, König F, Paech D, Tavakoli A, Laun FB, et al. Advanced Diffusion-Weighted Abdominal Imaging Qualitative and Quantitative Comparison of High and Ultra-High b-Values for Lesion Detection and Image Quality. *Invest Radiol*. 2020; 55(5):285–92. <https://doi.org/10.1097/RLI.0000000000000639> PubMed PMID: WOS:000534343800005. PMID: 32011572
35. Landis JR, Koch GG. The measurement of observer agreement for categorical data. *Biometrics*. 1977; 33(1):159–74. Epub 1977/03/01. PMID: 843571.
36. Metens T, Absil J, Denolin V, Bali MA, Matos C. Liver apparent diffusion coefficient repeatability with individually predetermined optimal cardiac timing and artifact elimination by signal filtering. *Journal of magnetic resonance imaging: JMRI*. 2016; 43(5):1100–10. Epub 2015/11/15. <https://doi.org/10.1002/jmri.25089> PMID: 26566777.
37. Xiang Z, Ai Z, Liang J, Li G, Zhu X, Yan X. Evaluation of Regional Variability and Measurement Reproducibility of Intravoxel Incoherent Motion Diffusion Weighted Imaging Using a Cardiac Stationary Phase Based ECG Trigger Method. *Biomed Res Int*. 2018; 2018:4604218. Epub 2018/06/01. <https://doi.org/10.1155/2018/4604218> PMID: 29850518; PubMed Central PMCID: PMC5932501.
38. Ichikawa S, Motosugi U, Tamada D, Wakayama T, Sato K, Funayama S, et al. Improving the Quality of Diffusion-weighted Imaging of the Left Hepatic Lobe Using Weighted Averaging of Signals from Multiple Excitations. *Magnetic Resonance in Medical Sciences*. 2019; 18(3):225–32. <https://doi.org/10.2463/mrms.mp.2018-0085> PubMed PMID: WOS:000503843200008. PMID: 30555108
39. Liao J, Lee J, Schroeder ME, Sirlin CB, Bydder M. Cardiac motion in diffusion-weighted MRI of the liver: artifact and a method of correction. *J Magn Reson Imaging*. 2012; 35(2):318–27. Epub 2011/10/01. <https://doi.org/10.1002/jmri.22816> PMID: 21959926; PubMed Central PMCID: PMC3252483.
40. Moulin K, Aliotta E, Ennis DB. Effect of flow-encoding strength on intravoxel incoherent motion in the liver. *Magn Reson Med*. 2019; 81(3):1521–33. Epub 2018/10/03. <https://doi.org/10.1002/mrm.27490> PMID: 30276853.
41. Laun FB, Demberg K, Nagel AM, Uder M, Kuder TA. On the Vanishing of the t-term in the Short-Time Expansion of the Diffusion Coefficient for Oscillating Gradients in Diffusion NMR. *Front Phys*. 2017; 5:56. doi: ARTN 56 <https://doi.org/10.3389/fphy.2017.00056> PubMed PMID: WOS:000415060100001.
42. Bruegel M, Gaa J, Waldt S, Woertler K, Holzapfel K, Kiefer B, et al. Diagnosis of hepatic metastasis: comparison of respiration-triggered diffusion-weighted echo-planar MRI and five t2-weighted turbo spin-echo sequences. *AJR American journal of roentgenology*. 2008; 191(5):1421–9. Epub 2008/10/23. <https://doi.org/10.2214/AJR.07.3279> PMID: 18941080.
43. Coenegrachts K, Delanote J, Ter Beek L, Haspelslagh M, Bipat S, Stoker J, et al. Improved focal liver lesion detection: comparison of single-shot diffusion-weighted echoplanar and single-shot T2 weighted turbo spin echo techniques. *Br J Radiol*. 2007; 80(955):524–31. Epub 2007/05/19. <https://doi.org/10.1259/bjr/33156643> PMID: 17510250.
44. Koh DM, Brown G, Riddell AM, Scurr E, Collins DJ, Allen SD, et al. Detection of colorectal hepatic metastases using MnDPDP MR imaging and diffusion-weighted imaging (DWI) alone and in combination. *European radiology*. 2008; 18(5):903–10. Epub 2008/01/15. <https://doi.org/10.1007/s00330-007-0847-z> PMID: 18193234.
45. Nasu K, Kuroki Y, Nawano S, Kuroki S, Tsukamoto T, Yamamoto S, et al. Hepatic metastases: diffusion-weighted sensitivity-encoding versus SPIO-enhanced MR imaging. *Radiology*. 2006; 239(1):122–30. Epub 2006/02/24. <https://doi.org/10.1148/radiol.2383041384> PMID: 16493012.
46. Parikh T, Drew SJ, Lee VS, Wong S, Hecht EM, Babb JS, et al. Focal liver lesion detection and characterization with diffusion-weighted MR imaging: comparison with standard breath-hold T2-weighted imaging. *Radiology*. 2008; 246(3):812–22. Epub 2008/01/29. <https://doi.org/10.1148/radiol.2463070432> PMID: 18223123.
47. Taouli B, Koh DM. Diffusion-weighted MR imaging of the liver. *Radiology*. 2010; 254(1):47–66. Epub 2009/12/25. <https://doi.org/10.1148/radiol.09090021> PMID: 20032142.